Selection of full Poincaré beams with higher robustness in turbulent atmosphere (*Invited*)

Liu Xueting[1,2,3], Zhai Yanwang[1,2,3], Fu Shiyao[1,2,3], Gao Chunqing[1,2,3*]

(1. School of Optics and Photonics, Beijing Institute of Technology, Beijing 100081, China;
2. Key Laboratory of Information Photonics Technology, Ministry of Industry and Information Technology, Beijing 100081, China;
3. Key Laboratory of Photoelectronic Imaging Technology and System Ministry of Education, Beijing 100081, China)

Abstract: Full Poincaré beams, as a more complicated class of novel structural beams, lead to impressive demonstrations recently in Free-Space Optical Communication (FSOC) due to the coupling of spin and orbital angular momentum in the cross section. However, a noteworthy limiting factor of FSOC system in this process is the varying atmospheric turbulence which results in beam expansion, drift, light intensity scintillation and other severe effects. Massive numerical simulations on turbulent atmospheric propagation of full Poincaré beams with C-point polarization, cylindrical vector beams with V-point polarization and homogeneous scalar polarized vortex beams through random phase screens were demonstrated. In this process, normalized correlation coefficient and mode purity were proposed to explore the robustness of full Poincaré beams on different locations of hybrid-order Poincaré sphere. The results show that full Poincaré beams with coordinates located in the southern hemisphere remain high robustness under weak and moderate turbulence (r_0=0.5 m, 0.125 m) compared with cylindrical vector beams and scalar vortex beams with similar topological charges and intensity distribution. While the dominant area shrinks to $2\sigma\in[-5\pi/32, 0]$ (latitude coordinates) under strong turbulence (r_0=0.056 m). These results will promote the selection of robust transmission media and the development of transmission quality in free-space communications with long-distance.

Key words: full Poincaré beams; atmosphere turbulence; higher robustness; hybrid-order Poincaré sphere

CLC number: O43 **Document code:** A **DOI:** 10.3788/IRLA20210242

湍流大气中高稳定性全庞加莱球光束模式选择 (特邀)

刘雪婷[1,2,3], 翟焱望[1,2,3], 付时尧[1,2,3], 高春清[1,2,3*]

(1. 北京理工大学 光电学院, 北京 100081;
2. 信息光子技术工业和信息化部重点实验室, 北京 100081;
3. 光电成像技术与系统教育部重点实验室, 北京 100081)

摘 要: 作为新型结构光束的一类,全庞加莱球光束因其横截面上自旋角动量和轨道角动量发生耦合,近年来在自由空间光通信领域内受到广泛关注。然而,传输信道中的大气湍流将产生诸如光束扩

收稿日期:2021−04−13; **修订日期:**2021−05−19

基金项目:国家自然科学基金 (11834001, 61905012); 国防基础科研计划 (JCKY2020602C007)

作者简介:刘雪婷, 女, 硕士生, 主要从事结构光场的传输及自适应校正方面的研究。

导师(通讯作者)简介:高春清, 男, 教授, 博士生导师, 博士, 主要从事新型激光器件与技术、光场调控技术、激光雷达技术等方面的研究。

展、漂移、光强闪烁等严重影响，进而限制光通信系统性能。结合随机相位屏，对具有“C”型偏振奇点的全庞加莱球光束、“V”型偏振奇点的柱矢量光束和均匀偏振的标量涡旋光束在湍流大气中的传播进行大量的数值模拟。归一化光强相关系数和模式纯度被用于研究杂合庞加莱球表面不同位置处表征的全庞加莱球的稳定性。结果表明，相较于具有相似偏振拓扑荷和光强分布的柱矢量光束以及标量涡旋光束而言，坐标位于南半球的全庞加莱球光束在弱湍流和中湍流 (r_0=0.5 m, 0.125 m) 下具有较高稳定性。而在强湍流下 (r_0=0.056 m)，优势区域缩小至 $2\sigma \in [-5\pi/32, 0]$(纬度坐标)。上述结果将为自由空间远距离通信中传输介质的选取提供重要依据并进一步促进通信质量的提升。

关键词： 全庞加莱球光束； 大气湍流； 高稳定性； 杂合庞加莱球

0 Introduction

Free-Space Optical Communication (FSOC) requires both diversity and robustness of the transmission medium in the free atmosphere channel. In practice, however, the space and time-varying refractive index fluctuations in turbulent atmosphere leads to beam expansion, drift, light intensity scintillation and other severe effects[1−2]. All issues above in turn lead to beam quality degradation and the decrease of bit error rate at the receiver. In recent years, Vector Vortex Beams (VVBs)[3] with the coupling of the helicoidal wavefront carrying Orbital Angular Momentum (OAM) and inhomogeneous polarization carrying Spin Angular Momentum (SAM) in the cross section, stand out in FSOC system due to multiple degrees of freedom for modulation[4−5]. The two typical VVBs are C-point polarization Full Poincaré Beams (FPBs)[6] and V-point polarization Cylindrical Vector Beams (CVBs), which have been proved to maintain information diversity and high robustness simultaneously compared with homogeneous polarization Scalar Vortex Beams (SVBs)[7−9]. In this process, the advantages of FPBs are particularly prominent. Wei et al.[10] demonstrated that FPBs significantly reduce the scintillation index compared to SVBs under certain conditions. Senthilkumaran et al.[11−12] presented experiments on propagation of C-point polarization FPBs through random phase fluctuations and investigated the diversity of speckle patterns generated by polarization components. Then the robustness of FPBs was verified experimentally based on the signal to noise ratio and scintillation index compared with V-point polarization CVBs. The above results give FPBs the possibility of achieving high robustness optical communication. However, most studies have focused only on FPBs located on the equator of Hybrid-Order Poincaré Sphere (HyOPS)[13], the non-equatorial region are poorly investigated. We are motivated to select a class of FPBs on HyOPS (characterized by latitude and longitude coordinates) that can achieve high robustness under different evaluation indexes.

In this manuscript, we demonstrate the high robustness region of C-point polarization FPBs on HyOPS compared with V-point polarization CVBs and homogeneous polarized SVBs. As well as Normalized Correlation Coefficient (NCC) and Mode Purity (MP) are firstly employed to evaluate optical performance of different latitude and longitude coordinates on HyOPS. The results demonstrate that C-point polarization FPBs achieve higher robustness when the latitude coordinates are regulated within a certain range according to different evaluate indexes, the order of FPBs and turbulence intensities. Under the settings of this article, both 2nd and 4th order FPBs located in the southern hemisphere are more advantageous under weak and moderate turbulence (r_0=0.5 m, 0.125 m). While the latitude coordinates corresponding to the dominant region shrink to $2\sigma \in [-5\pi/32, 0]$ under strong turbulence approximately (r_0=0.056 m).

1 Principles and concepts

1.1 Full Poincaré beams on hybrid-order Poincaré spheres

VVBs can be generated by the coherent superposition of two circularly polarized scalar Laguerre-Gaussian beams (LGBs) with orthogonal polarization

states and different topological charges. The light field can be represented as[14]

$$\left|\psi_{m,n}\right\rangle=\exp(il_p\varphi)\psi_L^n\exp\frac{-i(p\varphi+\theta_0)}{2}|L\rangle+\exp(il_p\varphi)\psi_R^m\exp\frac{i(p\varphi+\theta_0)}{2}|R\rangle \tag{1}$$

where ψ_L^n and ψ_R^m denote the radial light field of two polarization components with initial polarization direction θ_0 when φ=0, m and n are the topological charges of two components. $|L\rangle=(\mathrm{e}_x+i\mathrm{e}_y)/\sqrt{2}$ and $|R\rangle=(\mathrm{e}_x-i\mathrm{e}_y)/\sqrt{2}$ denotes the basis vector of left-hand and right-hand circularly polarization, respectively.

Any VVBs can be mapped to the hybrid-order Poincaré sphere and characterized by the polarization order p=(m-n)/2 and the Pancharatnam-Berry topological charge l_p=(m+n)/2. The HyOPS are mapped by representing the Stokes parameters S_j(j=0, 1, 2, 3) in the spherical Cartesian coordinates which are defined as[13, 15]

$$\begin{bmatrix}S_0\\S_1\\S_2\\S_3\end{bmatrix}=\begin{bmatrix}\left|\psi_R^m\right|^2+\left|\psi_L^n\right|^2\\2\left|\psi_R^m\right|\left|\psi_L^n\right|\cos\theta_0\\2\left|\psi_R^m\right|\left|\psi_L^n\right|\sin\theta_0\\\left|\psi_R^m\right|^2-\left|\psi_L^n\right|^2\end{bmatrix} \tag{2}$$

where 2θ=arctan(S_2/S_1) and 2σ=arcsin(S_3/S_0) represent the longitude and latitude coordinates of HyOPS ($2\sigma\in[-\pi/2,\pi/2]$, $2\theta\in[0,2\pi]$). It's worth noting that the HyOPS model has universality for FPBs, CVBs and SVBs. When n=0, $m\neq0$, the composite beams named full Poincaré beams, with C-point polarization singularities in cross section, have multiple polarization types (linear polarization, elliptic polarization and circular polarization) simultaneously (see Fig.1). The light fields here are represent as

$$\psi_{m,0}=\sin\left(\sigma+\frac{\pi}{4}\right)\mathrm{e}^{i\theta}E_{0m}(r,\varphi,z)|R\rangle+\cos\left(\sigma+\frac{\pi}{4}\right)\mathrm{e}^{-i\theta}E_{00}(r,\varphi,z)|L\rangle \tag{3}$$

where $E_{0m}(r, \varphi, z)$ and $E_{00}(r, \varphi, z)$ denote the light field of LGBs with topological charge m and fundamental Gaussian beam, respectively. When m=−n≠0, the HyOPS degenerates into the High-Order Poincaré Sphere (HOPS) which characterizes V-point polarization CVBs with single type polarization. If either m or n exists (beams located in north and south poles on HyOPS), SVBs are represented.

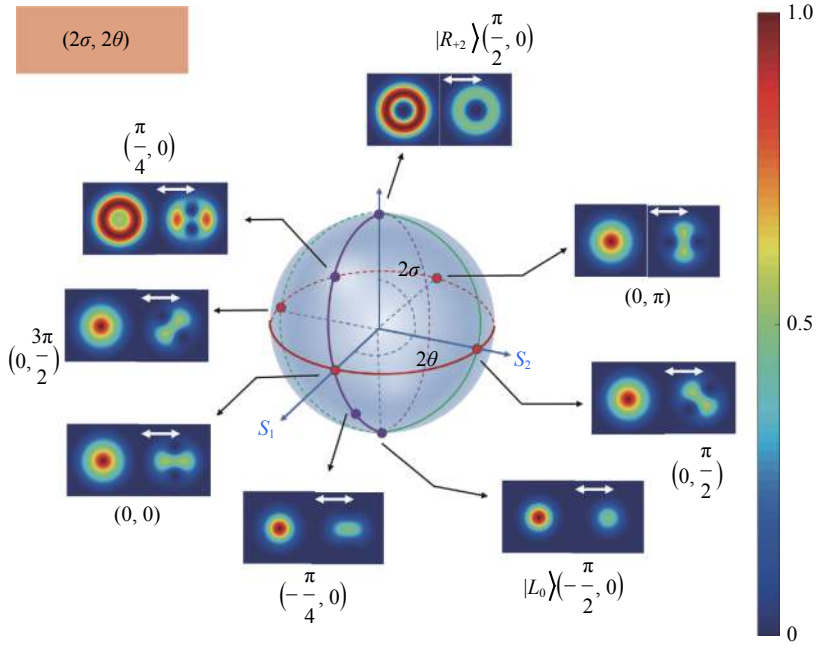

Fig.1 2nd order FPBs (m=2, n=0) with C-point polarization on HyOPS

1.2 Atmospheric turbulence model based on random phase screens

In this manuscript, the Atmospheric Turbulence (AT) channel is described by inserting a series of independent random phase screens with equal intervals Δz which conforming to sampling rules along the propagation direction. The initial light field goes through cycles (superposing random phase screen information —propagating certain distances forward under Fresnel diffraction theory—superposing another phase screen information) until it reaches the final distances[12]. The random phase screens mimic the atmosphere by using Zernike polynomials in which the disturbed wavefront $\phi(r,\ \varphi)$ caused by AT can be expressed as

$$\phi(r,\varphi)=\sum_{j=1}^{\infty}a_j\cdot Z_j(r,\varphi) \tag{4}$$

where $Z_j(r,\ \varphi)$ represents the Zernike polynomials of item j (up to 66 terms in our simulation); a_j is the coefficients of the j-th polynomial. The coefficients satisfy the covariance relationship based on Kolmogorov power spectrum[16].

$$\langle a_i,a_j\rangle=\left(\frac{D}{r_0}\right)^{5/3}\frac{2.269\ 8\cdot(-1)^{(n_i+n_j-2m_j)/2}}{\Gamma((n_j-n_i+17/3)/2)}\times \frac{[(n_i+1)(n_j+1)]^{1/2}\Gamma((n_i+n_j-5/3)/2)\delta_z}{\Gamma((n_i-n_j+17/3)/2)\Gamma((n_i+n_j+23/3)/2)} \tag{5}$$

where $\langle a_i,\ a_j\rangle$ represents the covariance between a_i and a_j; D is the beam diameter and r_0 is the atmospheric coherence length; n and m represent the radial degrees of freedom and angular frequencies of Zernike polynomials, respectively. $\Gamma(\xi)$ means Gamma function. $\delta_z=(m=m')\cap(\overline{parity(i,j)}\cup(m=0))$. The turbulence strength can be described by r_0. The smaller the value, the stronger the turbulence. The difference in coefficients and correspondence lead to the non-unique analytic form of Zernike polynomials which ensures the randomness of the phase screens successfully.

1.3 Atmospheric turbulence model based on random phase screens

We employ normalized correlation coefficient and mode purity to measure the evolution of intensity degradation and mode decomposition in turbulence.

Normalized Correlation Coefficient (NCC), to synthetically evaluate the degree of global intensity degradation and beam displacement, is defined as[17]

$$NCC=\frac{\int_0^1\int_{-\pi}^{\pi}I(r,\varphi,z)I_{\mathrm{id}}(r,\varphi,z)\,\mathrm{d}r\mathrm{d}\varphi}{\int_0^1\int_{-\pi}^{\pi}I_{\mathrm{id}}{}^2(r,\varphi,z)\,\mathrm{d}r\mathrm{d}\varphi} \tag{6}$$

where $I(r,\ \varphi,\ z)$ and $I_{\mathrm{id}}(r,\ \varphi,\ z)$ denote the intensity profile of turbulent beams and ideal beams. The greater the NCC is, the higher the correlation between the two, as well as the less AT distortion on optical channel.

Mode Purity (MP), obtained by calculating OAM spectrum, occupies a pivotal position in evaluating the performance of optical vortex. The complex amplitude of optical fields can be expanded in a linear space composed of harmonic functions $\exp(il\varphi)$ which described as[18]

$$u(r,\varphi,z)=\frac{1}{\sqrt{2\pi}}\sum_{l=-\infty}^{\infty}a_l(r,z)\exp(il\varphi) \tag{7}$$

where $a_l(r,z)=\frac{1}{\sqrt{2\pi}}\int_0^{2\pi}u(r,\varphi,z)\exp(-il\varphi)\mathrm{d}\varphi$. Then the relative power ratio of harmonic can be obtained by integrating the absolute value of the coefficient along the radius, and the MP can be obtained as

$$MP=\int_0^{\infty}|a_l(r,z)|^2r\mathrm{d}r\Big/\sum_{l=-\infty}^{\infty}\left[\int_0^{\infty}|a_l(r,z)|^2r\mathrm{d}r\right] \tag{8}$$

The higher the MP is, the more original components the distorted beam contains, and the less distortion the beam suffers.

2 Results and discussion

The parameters used in simulations are listed as follow. All propagation modes with wavelengths of λ= 1 550 nm maintain the consistent waist radius ω_0=10 cm. Weak, moderate and strong turbulence corresponded to r_0=0.5 m, 0.125 m, 0.056 m are selected, respectively. Multiple phase screens with the resolution of 1 080×1 080 keep Δz=100 m apart from each other, and the maximum propagation distance is 5 km. For statistical purposes,

each of the following data points are randomly tested 50 times and averaged to reduce the error.

2.1 Performance comparison between FPBs, CVBs and LGBs

In order to investigate the robustness performance of polarization singularity beams with different orders and polarization distributions compared with homogeneous polarized vortex beams in turbulent atmosphere, we introduce two classes based on the consistency of polarization topological charges and intensity distribution among C-point polarization FPBs, V-point polarization CVBs and LGBs. In each correspondence, FPB and CVB have the same polarization topological charge p and the same law of polarization direction change along the angular direction, as well as CVB and LGB have the same light intensity distribution in the cross section. According to Fig.2, comparison can be set up between 2nd order FPB (m=2, n=0), 1st order CVB (m=+1, n=−1) and 1st order LGB (m=+1) which defined as class 1 (low-order correspondence). Specifically, the comparison between 4th order FPB (m=4, n=0), 2nd order CVB (m=+2, n=−2) and 2nd order LGB (m=+2) is established as class 2 (high-order correspondence).

Firstly, set FPBs and CVBs position at (2σ, 2θ)=(0, 0) to study the most common patterns. Figure 3 and Fig.4 depicts that NCC and MP of 2nd and 4th order FPBs decrease gradually with the increase of propagation distances and turbulence intensities, which is accompanied by beam displacement, light intensity degradation and mode decomposition. All of which fits well with basic cognition. It is worth noting that the large topological charge of high order FPB is more likely to split into small topological charge. Meanwhile, the greater the value of m, the larger the hollow area of the right-handed circularly polarization component, which leads to the inadequate coupling with the fundamental mode near the center of light field. In turn, the performance of high-order FPB decreases.

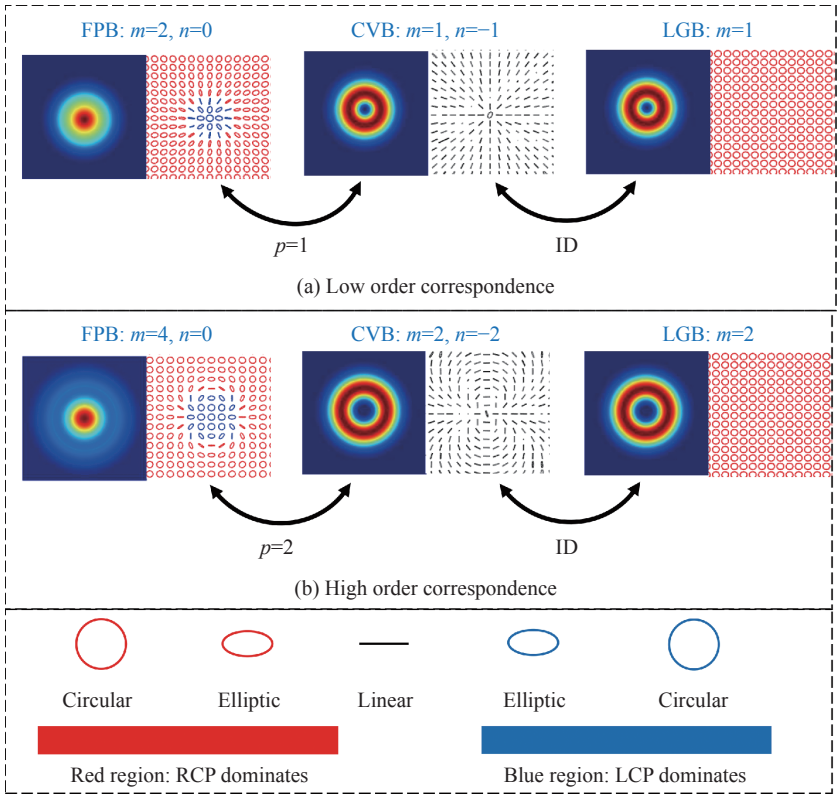

Fig.2 Polarization and intensity of beams in (a) low-order correspondence and (b) high-order correspondence. ID: intensity distribution; RCP: right-handed circular polarization; LCP: left-handed circular polarization

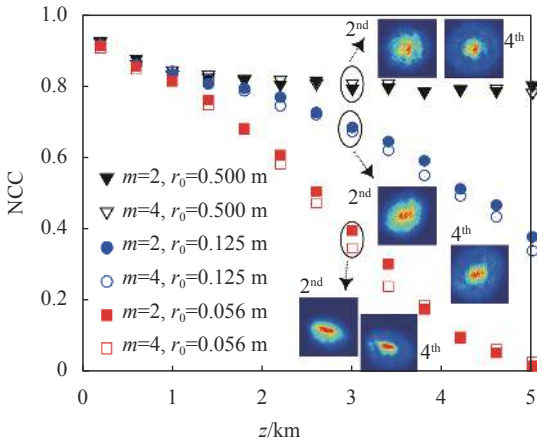

Fig.3 NCC of 2nd and 4th order FPBs at different propagation distances and turbulence intensities

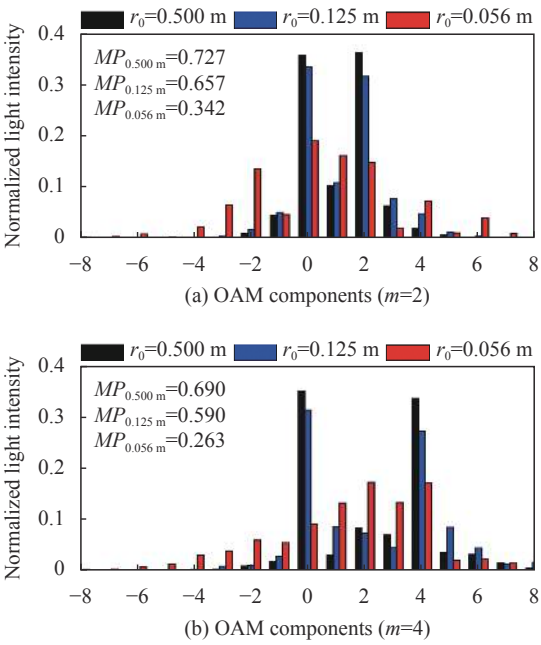

Fig.4 OAM components and mode purity of (a) the 2nd order FPB and (b) the 4th order FPB under different turbulence intensities at 3 km

Secondly, by comparing the NCC evolution of each beams of class 1 and 2 after passing through varied AT (see Fig.5), it is almost certain to argue that beams with inhomogeneous polarization characteristics have a stronger ability to resist the light intensity degradation and displacement, among which FPBs has a more obvious advantage. The NCC of FPBs, under the same condition, is significantly higher than that of CVBs and LGBs with the corresponding order. However, under strong

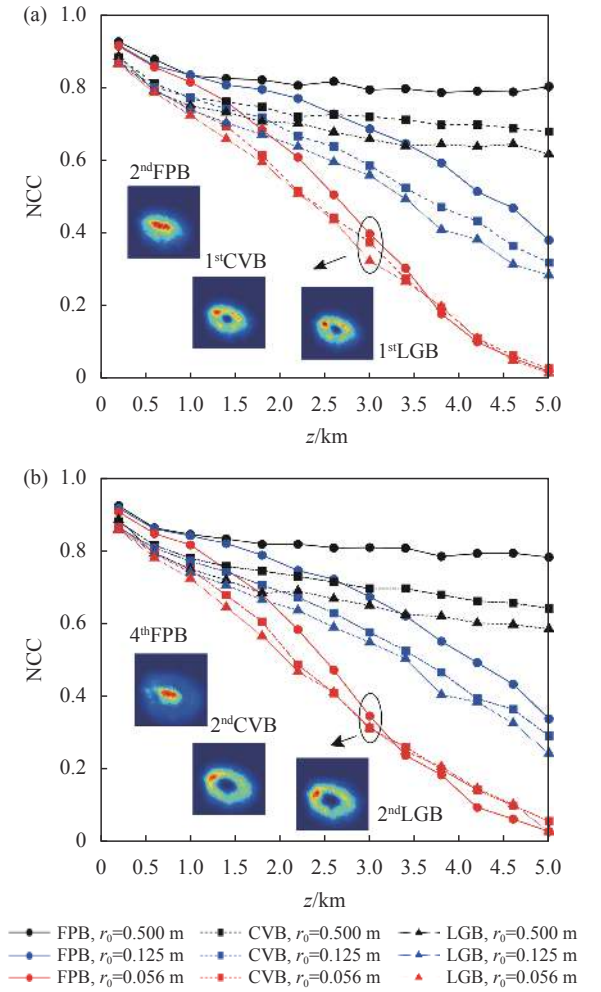

Fig.5 Comparison on NCC between (a) class 1 and (b) class 2 under different distances and turbulence intensities

turbulence and long transmission distances, the advantage will gradually disappear, as the NCC of three kinds of beams will tend to be the same at 3.5 km. More seriously, the curve of FPB is lower than that of others when the distance is greater than 3.5 km on class 2 according to Fig.5(b).

Part of similarities emerge about mode degradation which demonstrate a degree of robustness advantage of FPBs. According to Fig.6, in general, the MP performance of which processes inhomogeneous polarization (FPB and CVB) is better than that of scalar polarized LGB, and the advantage within low-order correspondence (class 1) is more apparent in this respect.

Different from the previous studies, which were mainly based on scintillation index and signal-to-noise

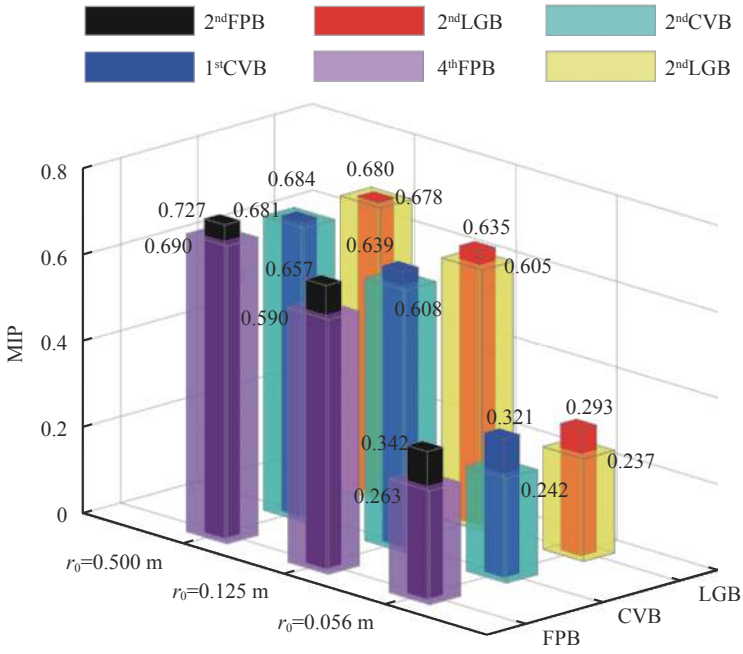

Fig.6 Comparison on MP between class 1 and class 2 under different turbulence intensities at 3 km

ratio, we adopt NCC and MP to verify the advantages of high robustness of FPBs on equator. The results are consistent with the previous results. We find that the tipping point for FPBs advantage is around 3 km, so it was necessary to keep the propagation distance at 3 km when discussing the following effects of longitude and latitude coordinates in order to avoid the interference caused by longer distance propagation.

2.2 The influence of longitude and latitude coordinates on FPBs and CVBs

Different longitude and latitude coordinates represent FPBs with different intensity and polarization distribution as show in Fig.1. We hope to find a class of FPBs with high robustness and map them to HyOPS to obtain their characteristics conveniently. After dividing semi-circle longitude line ($2\sigma\in[-\pi/2, \pi/2]$, $2\theta=0$) and full circle latitude line ($2\theta\in[0, 2\pi]$, $2\sigma=0$) by 64 equal parts, the sampling results are as follow.

Figure 7 shows that NCC and MP, under moderate turbulence, do not change greatly along the latitude line as well as both of them of FPBs are higher than that of CVBs which is consistent with the results in Section 2.1. The results indicates that longitude coordinates have no obvious effect on the performance of both FPBs and CVBs. As for latitude variation on FPBs ($2\theta=0$), the change of 2σ leads to the varied ratio of two superimposed components, resulting in great differences in spatial modes and light intensity distribution. CVBs avoid the effect because of the uniform distribution of light intensity, which can be embodied in broadly invariability of the NCC and MP. The remarkable fact is that the variation tendency of MP about FPBs is gradual decline (see Fig.8) while that of NCC emerges in sudden change region in Fig.8(a)-(c). In addition, different turbulence intensities make the abrupt change on NCC curves different, and then the intersection coordinates of NCC of FPBs and CVBs are also displaced.

At weak turbulence, generally, the NCC of FPBs in class 1 and class 2 which coordinates are located in the southern hemisphere is higher than that in the northern hemisphere as well as the overall change is relatively stable simultaneously (see Fig.8(a)). However, there is a trip point on curves of FPBs which goes up as the order of FPB increases. Under the current setting, the trip points of the 2nd to 4th order FPBs are located at $\pi/8$ and $3\pi/16$, respectively. The similar rule also appears in the case of moderate turbulence with trip points located at $9\pi/64$ and $11\pi/64$, respectively (see Fig.8(b)). Under strong

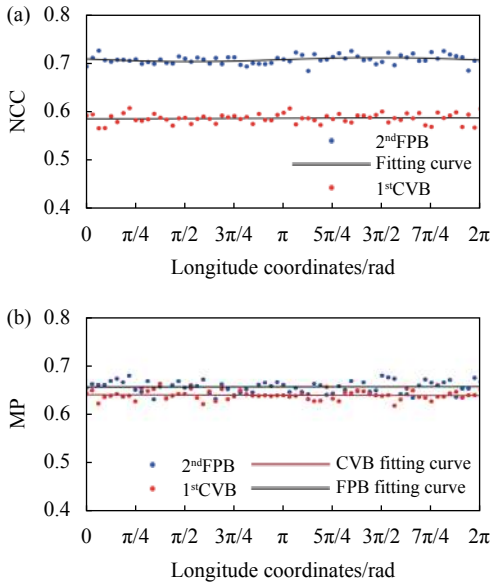

Fig.7 (a) NCC and (b) MP between 2nd order FPB and 1st order CVB with 2θ change (2σ=0, r_0 = 0.125 m)

turbulence, nevertheless, FPBs in the southern hemisphere lose its advantage in Fig.8(c). The closer it is to the north and south poles, the lower the NCC is. Meanwhile, the maximum value appears near 5π/64-11π/64 of latitude coordinates and the trip point still moves to the right simultaneously as the order increases. When 2σ>13π/64, the high robustness advantage of both 2nd and 4th order FPBs disappears with the similar NCC index compared to corresponding CVBs.

We think that the reason for the sudden drop of NCC curves is closely related to the distribution of light intensity under different latitude coordinates. We further divide semi-circle longitude line by 256 equal parts, and collect light intensity distributions of 2nd order FPB in radial direction (without AT). The results as shown in

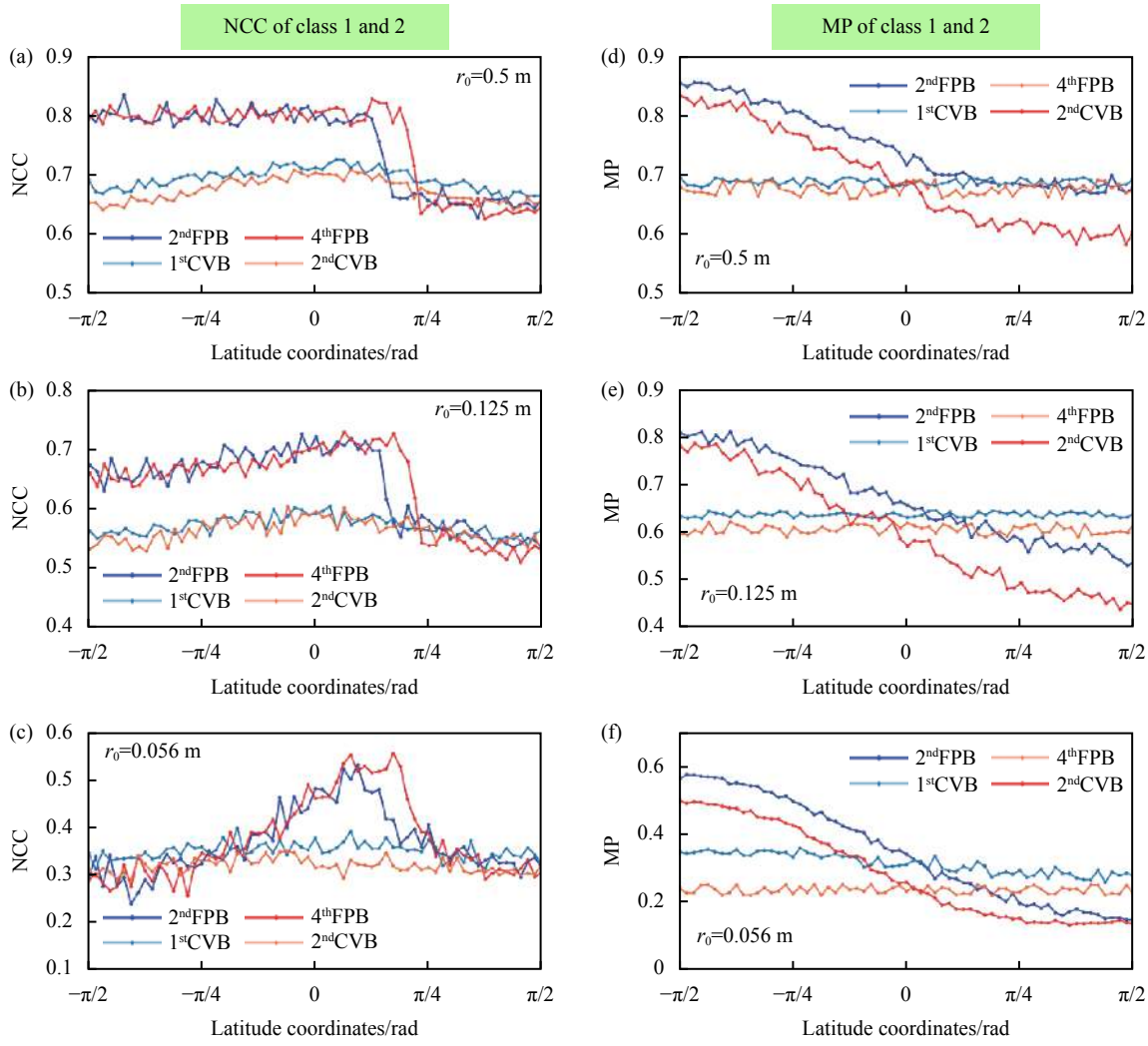

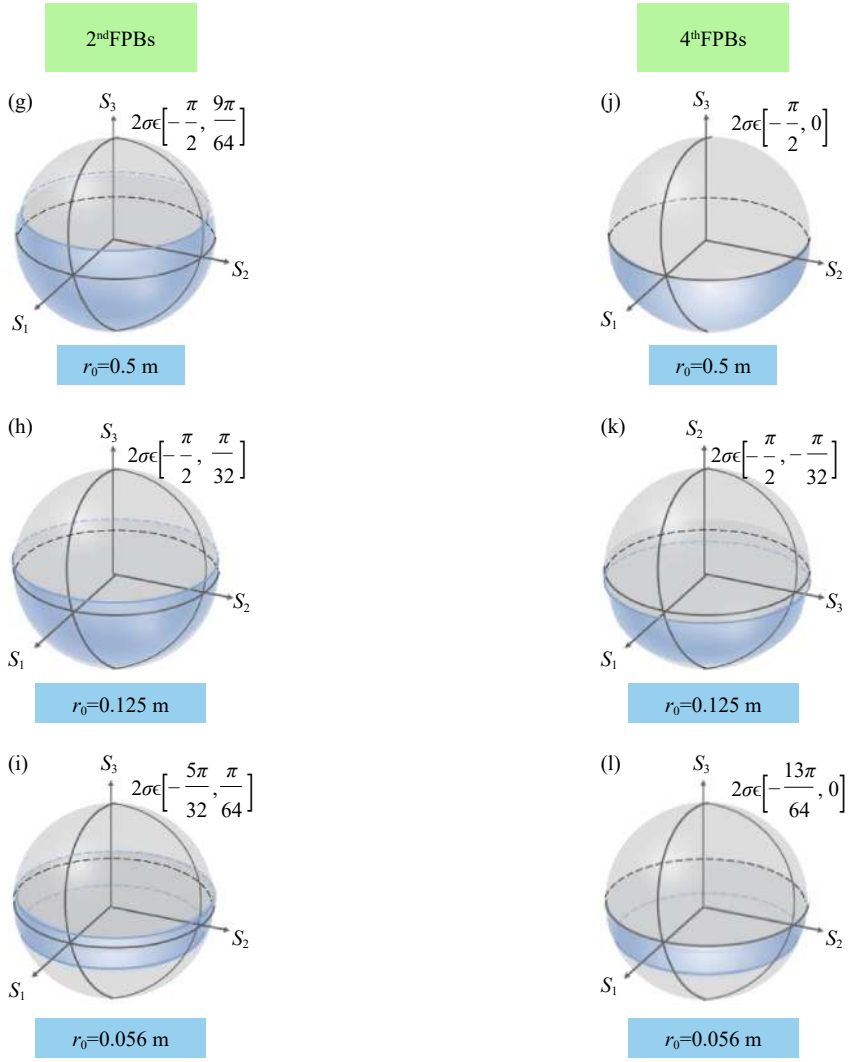

Fig.8 The first three rows: NCC and MP performance of class 1 and class 2 when changing coordinates along a latitude line with 2θ=0 under (a), (d) weak turbulence (r_0=0.5 m); (b), (e) moderate turbulence (r_0=0.125 m) and (c), (g) strong turbulence (r_0=0.056 m) respectively. The last three rows: the dominated longitude and latitude regions of (g), (h), (i) 2nd FPBs and (j), (k), (l) 4th FPBs on HyOPS under weak, moderate and strong turbulence

Fig.9. In the area of $2\sigma\in[\pi/8, \pi/4]$, the radial maximum light intensity increases rapidly. After reaching the peak, the position, where the maximum light intensity exists, begins to be separated from the center of beam. The phenomenon is accompanied by the reduction of light intensity in the central region which resulting in insufficient coupling between the two components used for superposition.

MP of FPBs overlap with that of corresponding CVBs near the equator which shows that FPBs are more robust when their coordinates are located in the southern

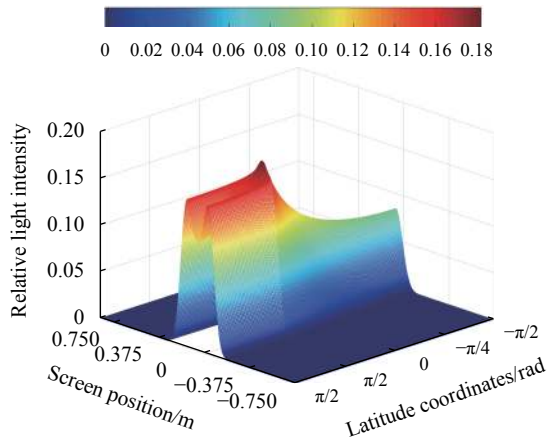

Fig.9 Light intensity distributions of 2nd order FPB in radial direction with 2σ change(without AT)

hemisphere (see Fig.8(d)-(f)). Different from the NCC tendency, low-order FPBs (2nd order FPBs) have a wider range of latitude coordinates with performance advantage compared with high-order FPBs (4th order FPBs). The dominant regions of the 2nd order FPBs are [−π/2, 9π/64], [−π/2, π/32] and [−π/2, π/64] under weak, moderate and strong turbulence respectively, while the area of 4th FPBs shrink to the southern hemisphere approximately.

We further extract dominated longitude and latitude regions of 2nd and 4th order FPBs from Fig.8(a)-(f) which satisfy the evaluation based on two indicators simultaneously. The results are shown in Fig. 8(g)-(l). As for class 1, under weak turbulence, 2nd order FPBs have higher robustness than 1st order CVBs when the latitude coordinate is less than 9π/64. While the area shrinks to $2\sigma\in$[−π/2, π/32] under moderate turbulence. However, under strong turbulence, the advantage is only valid when the latitude coordinate is in the range of −5π/32 to π/64. In class 2, the dominated latitude regions are $2\sigma\in$[−π/2, 0], [−π/2, −π/32] and [−13π/64, 0] under weak, moderate and strong turbulence, respectively.

Hence, FPBs with coordinates in the southern hemisphere can be selected as the transmission medium in the case of weak and moderate turbulence. Under strong turbulence, comprehensive consideration should be made according to the selected evaluation index.

3 Conclusion

In conclusion, combined with normalized correlation coefficient and mode purity, we have evaluated the propagation performance of C-point polarization full Poincaré beams, V-point polarization cylindrical vector beams and homogeneous polarized vortex beams in the communication link with atmospheric turbulence. All the simulation results have indicated that:

(1) The performance of FPBs decreases significantly with the increase of transmission distances, the order of FPBs and turbulence intensities.

(2) Full Poincaré beams can achieve high robustness in comparison with cylindrical vector beams and scalar vortex beams with corresponding order when the latitude coordinates are regulated within a certain range. Under weak turbulence (r_0=0.5 m), 2nd and 4th order FPBs have higher robustness than corresponding CVBs when the latitude coordinate is less than 9π/64 and 0. While the area shrinks to the [−π/2, π/32] and [−π/2, −π/32] under moderate turbulence (r_0=0.125 m), respectively. However, under strong turbulence (r_0=0.056 m), the advantage is only valid within a band as the latitude coordinate is in the range of [−5π/32, π/64] and [−13π/64, 0], respectively. In general, FPBs with coordinates located in the southern hemisphere can be selected under weak and moderate turbulence. While the area shrinks to the range of −5π/32 to 0 under strong turbulence.

To sum up, selecting full Poincaré beams as transmission medium as well as controlling their latitude and longitude coordinates on HyOPS can achieve higher robustness and information diversity of free-space optical communication system. Related research about these novel phenomena with mathematical and physical internal mechanisms are deserving of further investigation.

References:

[1] Zhai Y W, Fu S Y, Zhang J Q, et al. Turbulence aberration correction for vector vortex beams using deep neural networks on experimental data [J]. ***Optics Express***, 2020, 28(5): 7515-7527.

[2] Gao Chunqing, Zhang Shikun, Fu Shiyao, et al. Adaptive optics wavefront correction techniques of vortex beams [J]. ***Infrared and Laser Engineering***, 2017, 46(2): 0201001. (in Chinese)

[3] Rubinsztein-Dunlop H, Forbes A, Berry M V, et al. Roadmap on structured light [J]. ***Journal of Optics***, 2016, 19(1): 013001.

[4] Lavery M, Peuntinger C, Günthner K, et al. Free-space propagation of high-dimensional structured optical fields in an urban environment [J]. ***Science Advances***, 2017, 3(10): e1700552.

[5] Willner A E, Ren Y X, Xie G D, et al. Recent advances in high-capacity free-space optical and radio-frequency communications using orbital angular momentum multiplexing [J]. ***Philosophical Transactions A***, 2017, 375(2087): 20150439.

[6] Beckley A M, Brown T G, Alonso M A. Full Poincaré beams [J]. ***Optics Express***, 2010, 18(10): 10777-10785.

[7] Chen W, Haus J W, Zhan Q W. Propagation of vector vortex beams through a turbulent atmosphere [J]. ***Optics Express***, 2009, 17(20): 17829-17836.

[8] Cox M A, Rosales-Guzmán C, Lavery M, et al. On the resilience of scalar and vector vortex modes in turbulence [J]. ***Optics Express***, 2016, 24(16): 18105-18113.

[9] Yu J Y, Huang Y, Wang F, et al. Scintillation properties of a partially coherent vector beam with vortex phase in turbulent atmosphere [J]. ***Optics Express***, 2019, 27(19): 26676-26688.

[10] Wei C, Wu D, Liang C H, et al. Experimental verification of significant reduction of turbulence-induced scintillation in a full poincaré beam [J]. ***Optics Express***, 2015, 23(19): 24331-24341.

[11] Priyanka L, Senthilkumaran P, Khare K. Designer vector beams maintaining a robust intensity profile on propagation through turbulence [J]. ***Physical Review A***, 2018, 98: 023831.

[12] Lochab P, Senthilkumaran P, Khare K. Propagation of converging polarization singular beams through atmospheric turbulence [J]. ***Applied Optics***, 2019, 58: 6335-6345.

[13] Yi X N, Liu Y C, Ling X H, et al. Hybrid-order Poincaré sphere [J]. ***Physics Review A***, 2015, 91(2): 023801.

[14] Milione G, Sztul H I, Nolan D A, et al. Higher-order Poincaré sphere, Stokes parameters, and the angular momentum of light [J]. ***Physical Review Letters***, 2011, 107(5): 053601.

[15] Zhan Xiangkong, Li Zhengyong, Zhang Yi, et al. Radially polarized beam restructuring based on Stokes-vector measurement and interferometry [J]. ***Infrared and Laser Engineering***, 2017, 46(4): 0427002.

[16] Kolmogorov A N. The local structure of turbulence in incompressible viscous fluid for very large reynolds numbers [J]. ***Proceedings of the Royal Society A: Mathematical***, 1991, 434(1890): 9-13.

[17] Xie G D, Ren Y X, Huang H, et al. Phase correction for a distorted orbital angular momentum beam using a Zernike polynomials-based stochastic-parallel-gradient-descent algorithm [J]. ***Optics Letters***, 2015, 40(7): 1197-1200.

[18] Fu S Y, Zhai Y W, Zhang J Q, et al. Universal orbital angular momentum spectrum analyzer for beams [J]. ***PhotoniX***, 2020, 1: 19.